Directional information flow in patients with Alzheimer's disease. A source-space resting-state MEG study

M.M.A. Engels[a,*,1], M. Yu[b,1], C.J. Stam[b], A.A. Gouw[b], W.M. van der Flier[a,c], Ph. Scheltens[a], E.C.W. van Straaten[b], A. Hillebrand[b]

[a] Alzheimer Center and Department of Neurology, Neuroscience Campus Amsterdam, VU University Medical Center, Amsterdam, The Netherlands
[b] Department of Clinical Neurophysiology and MEG Center, VU University Medical Center, Amsterdam, The Netherlands
[c] Department of Epidemiology and Biostatistics, Neuroscience Campus Amsterdam, VU University Medical Center, Amsterdam, The Netherlands

ARTICLE INFO

ABSTRACT

In a recent magnetoencephalography (MEG) study, we found posterior-to-anterior information flow over the cortex in higher frequency bands in healthy subjects, with a reversed pattern in the theta band. A disruption of information flow may underlie clinical symptoms in Alzheimer's disease (AD). In AD, highly connected regions (hubs) in posterior areas are mostly disrupted. We therefore hypothesized that in AD the information flow from these hub regions would be disturbed. We used resting-state MEG recordings from 27 early-onset AD patients and 26 healthy controls. Using beamformer-based virtual electrodes, we estimated neuronal oscillatory activity for 78 cortical regions of interest (ROIs) and 12 subcortical ROIs of the AAL atlas, and calculated the directed phase transfer entropy (dPTE) as a measure of information flow between these ROIs. Group differences were evaluated using permutation tests and, for the AD group, associations between dPTE and general cognition or CSF biomarkers were determined using Spearman correlation coefficients. We confirmed the previously reported posterior-to-anterior information flow in the higher frequency bands in the healthy controls, and found it to be disturbed in the beta band in AD. Most prominently, the information flow from the precuneus and the visual cortex, towards frontal and subcortical structures, was decreased in AD. These disruptions did not correlate with cognitive impairment or CSF biomarkers. We conclude that AD pathology may affect the flow of information between brain regions, particularly from posterior hub regions, and that changes in the information flow in the beta band indicate an aspect of the pathophysiological process in AD.

1. Introduction

Patients with Alzheimer's disease (AD) clinically suffer from cognitive deficits in multiple cognitive domains, which is thought to be caused by intracellular tau inclusions (tangles) and extracellular accumulations of amyloid beta proteins (plaques) leading to synaptic loss, neuronal cell death and brain atrophy. The hippocampi, together with the posterior part of the default mode network (in particular the precuneus and posterior cingulate), are the most affected brain areas in AD. Besides these changes in brain structure, functional connections between distant brain areas are also affected in AD (e.g., refs. Alonso et al., 2011; Berendse et al., 2000; Besthorn et al., 1994; Engels et al., 2015; Franciotti et al., 2006; Wang et al., 2007; Zhang et al., 2009).

Functional connections can be evaluated by calculating the statistical interdependencies between time series of neuronal activity (Friston, 2011). It has been shown consistently, using different imaging modalities, that the changes in functional connectivity in AD depend on the brain regions involved: while mainly the posterior regions show increased connectivity, decreased functional connectivity seems to be much more widespread throughout the brain (Crossley et al., 2014; Engels et al., 2015; Engels et al., 2017; Greicius et al., 2004).

Magnetoencephalography (MEG) can be used to study disease related changes in AD. MEG is reference free, and its large number of sensors allows for sophisticated spatial filtering to accurately reconstruct neuronal activity for predefined cortical brain areas (Baillet et al., 2001; Hillebrand et al., 2005, 2012; Hillebrand et al., 2016a, 2016b). We have recently used this approach to reliably reconstruct oscillatory activity within the hippocampi of AD patients (Engels et al., 2016). The hippocampus has also been shown to function as a hub in the network (Battaglia et al., 2011; Yu et al., 2017), alongside the posterior regions. MEG can also be used to study the direction of information flow in brain networks, as we have recently shown in a group

of healthy subjects (Hillebrand et al., 2016a). This study revealed an anterior-to-posterior pattern in the theta band (4–8 Hz) while a posterior-to-anterior pattern was observed in the alpha1 (8–10 Hz), alpha2 (10–13 Hz), and beta bands (13–30 Hz). These directed connectivity patterns may be a result of underlying network topology, e.g. hub status of a region (Moon et al., 2015). Moon et al. (2015) demonstrated in an electroencephalography (EEG) study that hubs have a more receiving role in the network compared to non-hubs. These results may have been affected by their reference choices (a common problem in EEG). Moreover, their measures of directionality were based on phase differences, which may provide misleading estimates of directionality (see Hillebrand et al., 2016a). However, the exact relationship between hub-status and preferred direction of information flow is as yet unclear. Using EEG, two studies have reported disrupted information outflow from the posterior regions to anterior regions in AD patients (Babiloni et al., 2009; Dauwan et al., 2016), which confirms the hypothesis of an affected pattern of information flow in the large-scale brain networks. However, the patterns of information flow reconstructed from EEG data are strongly dependent on the reference choice and should therefore be interpreted with care (Guevara et al., 2005). Evaluating the information flow using MEG discards the reference problem and allows for more accurate source-estimation, which is crucial for a better understanding of disease mechanism in AD.

We hypothesized that the dominant posterior-to-anterior pattern of information flow seen in healthy controls would be disrupted in AD patients. In particular, we expected that in higher frequency bands the outflow from posterior regions would be reduced due to damage in posterior hub regions, and that in the theta band the outflow from the hippocampi would be reduced. This hypothesis was tested by comparing the directionality of information flow for cortical and sub-cortical regions, as reconstructed from resting-state MEG data, between healthy controls and patients with AD.

2. Methods

2.1. Subjects

Subjects used in this study have been previously described (Engels et al., 2016; Yu et al., 2017). In summary, 27 patients with probable AD with an early onset (age: 60.6 ± 5.4 years) from the Amsterdam Dementia Cohort in the Alzheimer Center of the VU University Medical Center were included. All patients fulfilled NIA-AA criteria for probable AD (McKhann et al., 2011). AD patients were assessed according to a standard diagnostic workup for dementia screening including an informant-based history of the patient (if available), physical-, neurological and cognitive examinations (including the mini-mental state examination (MMSE)), laboratory tests (including cerebrospinal fluid (CSF) amyloid and tau), structural brain imaging, and EEG. Diagnoses were made in a multidisciplinary consensus meeting. Patients gave written informed consent for use of their clinical data for research purposes (van der Flier et al., 2014). Exclusion criteria for participation in this study were: an active psychiatric or other neurologic disorder, MMSE-score below 18, or age above 70 years. In addition to the patient group, we included 26 out of 31 non-demented controls who responded to an advertisement in a national newspaper. After a telephone interview to exclude neurological or psychiatric disorders, subjects underwent neuropsychological testing, MRI of the brain and an MEG recording. One volunteer was excluded due to a meningioma found on the MRI; four volunteers were excluded due to poor performance on the neuropsychological tests. The local Ethics Committee approved the study and all participants gave written informed consent prior to participation.

2.2. Data acquisition

MEG recordings were obtained one to several hours before or more

than one week after the MRI-scan in order to avoid artifacts due to, for example, magnetized dental material. The resting-state MEG recordings consisted of a 5 min eyes-closed condition, followed by 2 min eyes open, and again 5 min eyes-closed. In this protocol, to ensure that the subjects stayed awake during recording, we asked them to open their eyes for 2 min after 5 min eyes-closed recording. To avoid potential confounders due to eye-blinks during the eyes-open condition, and because EEG parameters during the eyes-closed condition are more stable over sessions (Corsi-Cabrera et al., 2007), we only analysed the second five-minute eyes-closed data segment (van Diessen et al., 2015). The data were sampled at 1250 Hz, and an online anti-aliasing (410 Hz) and a high-pass filter (0.1 Hz) were used. The head position relative to the MEG sensors was recorded continuously using the signals from five head-localization coils. The head-localization coil positions were digitized, as well as the outline of the participant's scalp (~500 points), using a 3D digitizer (Fastrak, Polhemus, Colchester, VT, USA). This scalp surface was used for co-registration with the patient's MRI scan (see below). The data were spatially filtered offline using the temporal extension of Signal Space Separation (tSSS) (Taulu and Simola, 2006; Taulu and Hari, 2009), using MaxFilter software (Elekta Neuromag Oy, version 2.2.10). Channels containing excessive artifacts were manually discarded after visual inspection of the data by one of the authors (ME) before estimation of the SSS coefficients. The number of excluded channels varied between one and twelve. After fine-tuning for acquisition conditions at our site, the tSSS filter was used to remove noise signals that SSS would fail to discard, typically from noise sources near the head, using a subspace correlation limit of 0.9 (Medvedovsky et al., 2009; Hillebrand et al., 2013) and a sliding window of 10 s. Typical artifacts were due to (eye) movements, swallowing, dental prosthetics, or drowsiness, although the subjects were instructed to stay awake and reduce eye movements during the MEG recording.

CSF samples were obtained by lumbar puncture using a 25-gauge needle, and collected in 10-mL polypropylene tubes (Sarstedt, Nümbrecht, Germany) according to consensus protocols (Teunissen et al., 2009) only in the AD patients. Amyloid-beta 1–42, total tau, and p-tau were measured with commercially available ELISAs (Duits et al., 2015).

Structural MRI scans were made for all participants. For one AD patient, a computer tomography (CT) scan was obtained instead of an MRI because of insufficient quality of the MRI. For all participants, the outline of the scalp on the structural scans was extracted. The sphere that best fitted the scalp surface was used as a volume conductor model for the beamformer analysis described below. Co-registration of the MEG data with the structural scans was achieved using surface matching software, resulting in an estimated co-registration accuracy of approximately 4 mm (Whalen et al., 2008). The result of the co-registration between the MEG- and the MRI/CT scalp surfaces was visually inspected.

2.3. Source localization

In order to obtain source localized activity for all brain regions, we applied an atlas-based beamformer approach (Hillebrand et al., 2012), which projects the sensor signals to the 78 cortical regions-of-interest (ROIs) (Gong et al., 2009), and 12 sub-cortical regions of the automated anatomical labeling (AAL) atlas (Tzourio-Mazoyer et al., 2002) (Table S1). Details about the beamformer are similar as described in (Hillebrand et al., 2016a): The beamformer (Elekta Neuromag Oy; version 2.1.28) sequentially reconstructs the activity for each centroid by selectively weighting the contribution from each MEG sensor to a centroid's time series. The beamformer weights are based on the data covariance matrix and the forward solution (lead field) of a dipole source at the centroid location (Hillebrand et al., 2005; Robinson and Vrba, 1999; van Veen et al., 1997), where the optimum dipole orientation was obtained using the eigendecomposition approach described by Sekihara and colleagues (Sekihara et al., 2004; using a unity

matrix as estimate for the noise covariance matrix). A time window of, on average, 277 s (range 105–435 s) was used to compute the data covariance matrix. Singular value truncation was used when inverting the data covariance matrix to deal with the rank deficiency of the data after SSS (~70 components). The time series for the 90 ROIs were obtained by projecting the broad band (0.5–48 Hz) MEG data through the normalized (Cheyne et al., 2007) broadband beamformer weights for each ROI.

2.4. Data selection

For each subject, twenty artifact-free epochs of 4096 samples (3.2768 s) were selected by one of the authors [ME]. A second researcher [IN, in acknowledgements] independently evaluated a sub-set of the selected epochs for quality. Epochs without consensus were replaced by new epochs. Selected epochs were converted to ASCII-files and imported into an in-house developed software package (BrainWave version 0.9.125.4.1, CS. Software available at: http://home.kpn.nl/stam7883/brainwave.html). The ROI time series were digitally filtered in the classical EEG frequency bands using a fast Fourier transform that does not distort the phases: delta (0.5–4 Hz), theta (4–8 Hz), lower alpha (8–10 Hz), upper alpha (10–13 Hz), beta (13–30 Hz), and gamma (30–48 Hz).

2.5. Phase transfer entropy

The direction of information flow between ROIs was estimated using the phase transfer entropy (PTE), which was introduced by Paluš and Stefanovska (2003), and thoroughly evaluated by Lobier and colleagues (Lobier et al., 2014). The instantaneous phase time-series were estimated using the Hilbert transform (Rosenblum et al., 1996). We used the implementation as described in (Hillebrand et al., 2016a): PTE quantifies the information flow between time series on the basis of phase information. For the PTE the time series of the phases are used as input for the transfer entropy (TE) (Schreiber, 2000), which is a specific version of the Kullback-Leibler entropy (Kullback and Leibler, 1951) or the conditional mutual information (Paluš and Stefanovska, 2003; Paluš and Vejmelka, 2007; for review see Hlaváčková-Schindler et al., 2007). As an information-theoretic measure, the TE characterizes the information transfer between time series. The TE can be easily understood in terms of uncertainty: a source signal has a causal influence on a target signal if the uncertainty of the target signal conditioned on both its own past and that of the source signals is smaller than the uncertainty of the target signal conditioned only on its own past. If the uncertainty of a target signal Y at a delay δ is expressed in terms of Shannon Entropy (Shannon, 1948), then the TE from source signal X to target signal Y can be expressed as

$$TE_{xy} = \sum p(Y_{t+\delta}, Y_t, X_t) \log\left(\frac{p(Y_{t+\delta} \mid Y_t, X_t)}{p(Y_{t+\delta} \mid Y_t)}\right) \tag{1}$$

where the definition for Shannon Entropy, $H(Y) = -\Sigma p(Y)\log p(Y)$, was used, and the sum runs over all discrete time steps t.

For observed data, estimation of the probabilities in Eq. (1) is time-consuming and requires fine-tuning of several parameters (Wibral et al., 2011). To solve these problems, Staniek and Lehnertz proposed to estimate transfer entropy by converting observed time series into sequences of symbols (Staniek and Lehnertz, 2008). In the same spirit, time series can be described in terms of their amplitudes and instantaneous phases (Rosenblum et al., 2001), following which transfer entropy can be estimated from the time series of the instantaneous phases (PTE), at low computational cost (Paluš and Stefanovska, 2003; Lobier et al., 2014). Dropping the subscript t for clarity, and to speed-up the computations, we computed the PTE as:

$$PTE_{xy} = \sum p(Y_\delta)p(Y)p(X) \log\left(\frac{p(Y_\delta \mid Y, X)}{p(Y_\delta \mid Y)}\right) \tag{2}$$

where the probabilities are obtained by building histograms of occurrences of single, pairs or triplets of phase estimates in an epoch (Lobier et al., 2014). In Eq. (2), we assumed that the probability distribution of source signal X is independent with that of target signal Y, so $p(Y_\delta, Y, X) = p(Y_\delta)p(Y)p(X)$. This assumption has no influence on the information flow patterns and could speed up the computation time (Prokopenko and Lizier, 2014). The number of bins in the histograms was set as $e^{0.626 + 0.4\ln(N_s)} - \delta - 1)$ (Rosenblum et al., 2001), and the prediction delay δ was set as $(N_s \times N_{ch}) / N_\pm$, with N_s and N_{ch} the number of samples and channels (ROIs), respectively, and $N_\pm$ the number of times the phase changes sign across time and channels. Previous results have demonstrated that the choice of the delay does not influence the results (Lobier et al., 2014). The prediction delays for different frequency bands are given in Table S5.

Finally, because the PTE does not have a meaningful upper bound (Lobier et al., 2014), and to reduce biases, i.e., the effect of having (small) nonzero PTE values in situations when there is no actual information flow, we normalized the PTE,

$$dPTE_{xy} = \frac{PTE_{xy}}{PTE_{xy} + PTE_{yx}} \tag{3}$$

The value of $dPTE_{xy}$ ranges between 0 and 1. When information flows preferentially from time series X to time series Y, $0.5 < dPTE_{xy} \leq 1$. When information flows preferentially towards X from Y, $0 \leq dPTE_{xy} < 0.5$. In the case of no preferential direction of information flow, $dPTE_{xy} = 0.5$.

Eq. (2) is a modified version of the PTE as introduced by Lobier et al. (2014). To test the effect of making the assumption of independent probability distributions (for the joint probability term only), we also computed dPTE using Eq. (1) directly to compute the PTE. Eq. (3) and permutation testing with FDR correction (see Statistical analysis) was used again to compare the dPTE values between AD and control groups. The comparison of the results between dPTE and the modified version of dPTE, as by Lobier et al., 2014, can be found in the Supplementary Material, which shows that both approaches give very similar results.

The dPTE value for all pairwise ROIs was computed, forming a dPTE matrix, as well as the regional dPTE values, i.e. the average dPTE for each ROI. The regional dPTE values were computed by averaging all pairwise dPTE values from one ROI to all the other ROIs, and obtained one regional dPTE value for each of the 90 ROIs. This was repeated for all epochs in each frequency band, and for all subjects. The regional dPTE values indicate that on average a brain area is a driver ($0.5 < dPTE \leq 1$) or receiver ($0 \leq dPTE < 0.5$), relative to other areas.

To establish whether there was a consistent pattern of information flow in the MEG networks, a posterior-anterior index (PAx) (Hillebrand et al., 2016a) was calculated as follows:

$$PAx = \{\overline{dPTE}\}_{posterior} - \{\overline{dPTE}\}_{anterior} \tag{4}$$

where the dPTE was averaged over a set of anterior and posterior regions, respectively (see Table S1 for the definitions of anterior, central and posterior regions). PAx was normalized by the absolute maximum PAx value that could have been obtained with the dPTE values for these channels, respectively. A positive PAx indicates posterior-to-anterior information flow, and negative PAx anterior-to-posterior information flow.

To investigate whether there is different information flow from central to anterior regions and from central to posterior regions between AD and HCs, we also computed a central-to-anterior index (CAx) and a central-to-posterior index (CPx) for both groups. These results can be found in the Supplemental materials.

2.6. Statistical analysis

IBM SPSS Statistics 20.0 for mac was used for statistical analyses of the subjects' demographics. Differences between groups in age, MMSE and education were tested using unpaired Student's *t*-tests, while gender differences between groups were tested using a chi-square test.

For each frequency band separately, we used permutation tests to compare group-level 90 regional dPTE values between the two diagnostic groups, using the following approach:

1. Average the regional (AAL ROI) dPTE values for AD and control groups over all the epochs;
2. Compute the observed absolute difference between the group-level regional dPTEs of AD, and control groups;
3. Permute the group assignments of the individuals' dPTE matrices for AD and control groups (the epochs for the same subjects were always permuted together);
4. Repeat steps 1 to 3 to obtain 50,000 permutations of absolute differences for AD and control groups.

The observed absolute difference was tested against the sampled distribution in order to obtain a *p*-value. The *p*-values of pairwise comparisons were corrected by the false discovery rate (FDR) (Benjamini and Hochberg, 1995). The FDR-corrected *p*-values were considered to be significant at $p < 0.05$. Spearman correlation coefficients were calculated between the regional dPTE values of ROIs that showed significant differences between groups and MMSE scores, as well as protein biomarkers (CSF amyloid and tau).

We repeated the analyses for the individual dPTE values between all pairs of ROIs (i.e. the individual dPTE values were used in step 1) above, instead of the regional dPTE values, for which we included all individual connections of the upper triangular part of the dPTE matrix into the permutation test. Again, the permutations tests were FDR corrected. We only considered the frequency bands that had shown significantly different regional dPTE values between the groups.

The dPTE values for 90 ROIs were computed for AD and controls, respectively. The observed PAx value was computed for the averaged dPTE values for each group and the observed absolute difference between PAx values for two groups were computed. Significance of the group difference in PAx value was estimated using permutation testing, where dPTE values were permuted between groups, after which the absolute differences of PAx values were re-computed. This was repeated 50,000 times to build a distribution of permuted absolute difference of PAx values against which the observed absolute difference of PAx values was tested ($p < 0.05$).

The CPx and CAx values were compared between AD and controls using the same permutation procedure as described above for the PAx.

3. Results

3.1. Demographics

Characteristics of the healthy controls and patients with AD are presented in Table 1. Age ($t(51) = -0.82$, $p = 0.673$), education ($t(39) = -2.58$, $p = 0.462$), and gender ($c^2(1, 53) = 0.50$, $p = 0.587$) did not differ between groups, while MMSE scores were lower in AD patients than controls ($t(51) = -9.82$, $p < 0.001$).

3.2. Regional information flow

The beta band was the only frequency band showing differences in dPTE between patients and controls (Fig. 1). Fig. 1A reveals a dominant pattern of posterior-to-anterior information flow for healthy controls. In AD patients (Fig. 1B), this characteristic posterior-to-anterior pattern was disrupted, showing significantly lower mean dPTE values mainly in occipital (MOG.L and MOG.R, CAL.L and CAL.R, CUN.L and CUN.R,

Table 1

Subject characteristics. Abbreviations: Aβ42 = amyloid-β42; CSF = cerebrospinal fluid; F = number of female subjects; M = number of male subjects; MMSE = Mini-Mental State Examination; N = number of subjects; n.a. = not available; p-tau = tau phosphorylated at threonine 181; SD = standard deviation.

	AD patients	Healthy controls
N	27	26
Mean age (SD)	60.6 (5.4)	61.8 (5.5)
Gender (F/M)	12/15	14/12
Mean MMSE score (SD)	23.4 (2.6)**	28.9 (1.0)
Mean educational score (SD)[a]	4.84 (1.06)	5.71 (0.91)
Mean CSF Aβ$_{42}$ (range, pg/mL)	509 (324–674)	n.a.
Mean CSF tau (range, pg/mL)	715 (307–1677)	n.a.
Mean CSF p-tau (range, pg/mL)	83 (44–173)	n.a.

** $p < 0.01$.
[a] Level of education was rated according to Verhage (1964).

SOG.R), but also in parietal (PCUN.R), and temporal (FFG.L) regions, and significantly higher mean dPTE values in prefrontal (REC.L, ORBsupmed.L and ORBsupmed.R, ORBmid.R) and temporal regions (TPOsup.L) ($p < 0.05$) (Fig. 1C). The disruption of posterior-to-anterior information flow in AD patients was also quantified by the significantly lower ($p = 0.004$) PAx index in AD patients (PAx = 0.3689) compared to healthy controls (PAx = 0.5870). In comparison with controls (CPx = −0.3459), AD patients (CPx = 0.2238) showed a more central-to-posterior information flow characterized by significantly higher CPx ($p < 0.001$); AD (CAx = 0.4383) and control groups (CAx = 0.4161) showed similar central-to-anterior information flow ($p = 0.73$). Fig. S1 shows the results for the delta, theta, lower alpha, upper alpha and gamma band, which did not reveal significant differences between the two groups.

3.3. Information flow between regions

Fig. 2A and B show the dPTE matrices in the beta band for the healthy controls and AD patients, respectively. Abbreviations can be found in Table S1. From these figures it is clear that the dPTE values for the AD patients show less variation, and are more centered around the equilibrium value of 0.5, i.e. no preferred direction of information flow, compared to the controls. In controls (Fig. 2C), clear patterns of higher left and right parieto-occipital dPTE values can be observed. The strongest information flow was from posterior regions, including the (primary) visual areas and posterior parts of the default mode network (DMN), to anterior cingulate, frontal, and temporal regions. In contrast, in the AD patients, the global posterior-to-anterior information flow was disrupted (Fig. 2D). Specifically, the outgoing connections in AD patients started in left central brain areas (postcentral gyrus) and projected to the frontal, parietal and occipital regions; and also started in the right central regions (postcentral gyrus) and projected to the right frontal and temporal regions. Fig. S4 shows that, in the beta band, the strongest information flow in controls was between occipital-/parietal-/central regions and frontal regions, whereas in AD patients the strongest information flow was between central to frontal-/occipital-/temporal-/limbic regions.

The significant differences between the dPTE matrices in AD and controls are shown in Fig. 3 for the beta band. Fig. 3A shows that the information flow between posterior regions and frontal regions was decreased in AD patients, including occipital-to-frontal, occipital-to-temporal, parietal-to-frontal, parietal-to-temporal and occipital-to-limbic (limbic system: subcortical and cingulate gyrus) connections ($p < 0.05$). The connections with the most significant group differences ($p < 0.0001$) are displayed in Fig. 3B and described in Table S2. The most significant connections with lower dPTE values in AD patients were located in multiple occipital regions (SOG.L, SOG.R, MOG.L, MOG.R, CAL.L, CAL.R, CUN.L) and one temporal region (FFG.L) and connected to frontal regions (REC.R, ORBsup.R, ORBsupmed.R,
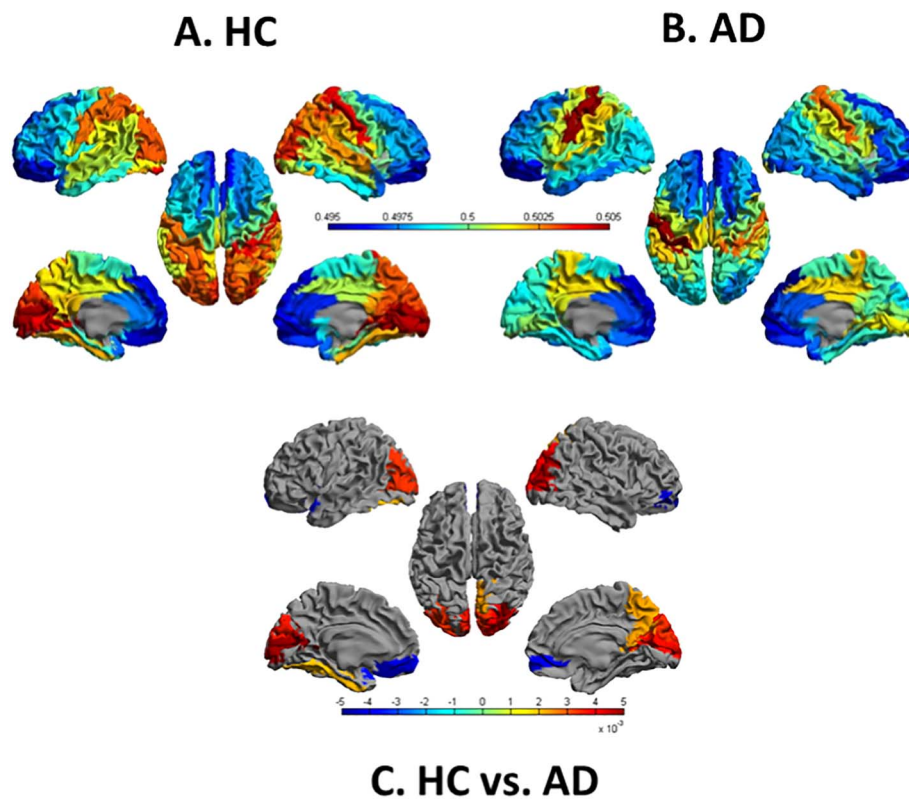
Fig. 1. Disrupted mean dPTE in AD patients in the beta band. Mean dPTE for the 78 cortical AAL ROIs only, displayed as a color coded map on a template mesh for healthy controls (HC) (A) and AD patients (B). (C) Cortical surface representation of the regions that demonstrated significant between-group difference in mean dPTE; group-level permutation tests with FDR correction ($p < 0.05$). Hot and cold colors indicate whether the mean dPTE was significantly higher or lower in controls than in AD patients, respectively; dPTE for regions in grey were not significantly different between controls and AD patients. The color bar in (C) denotes the mean difference of the dPTE values between HC and AD groups for the significant ROIs. (For interpretation of the references to color in this figure legend, the reader is referred to the web version of this article.)
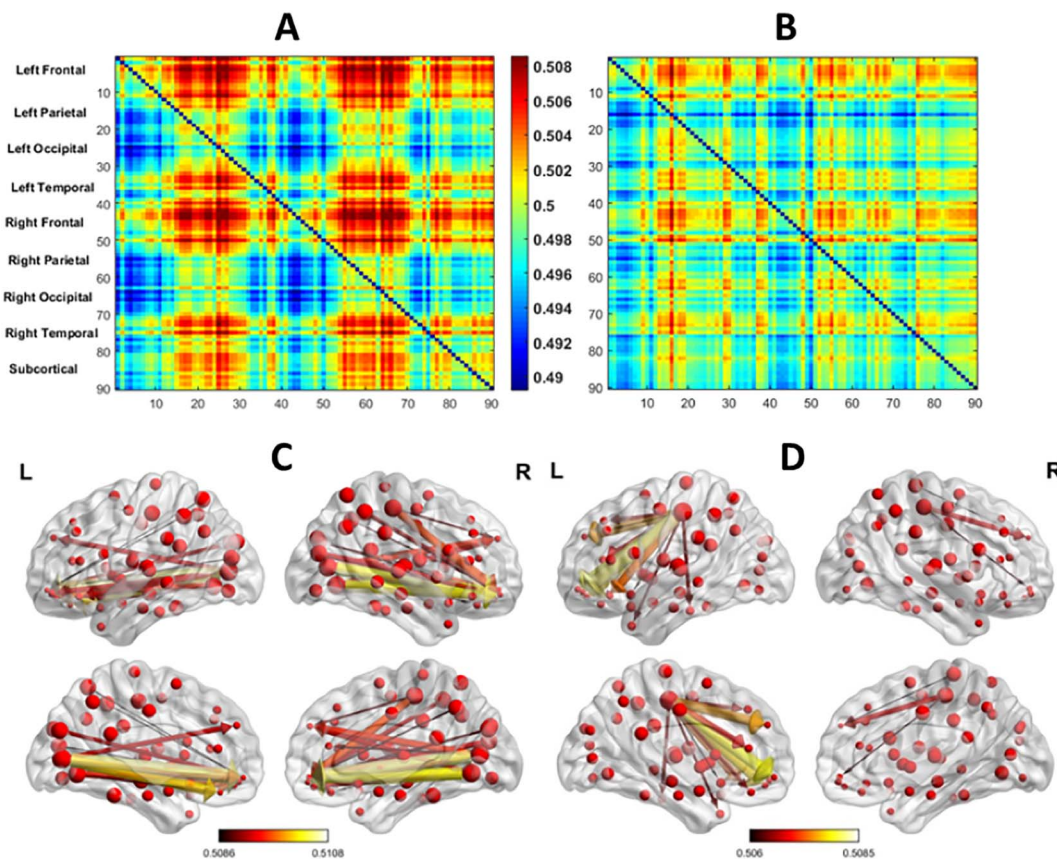
Fig. 2. Direction of information flow patterns in the beta band. Mean dPTE matrices for controls (A) and AD patients (B). Preferred direction of information flow of the strongest senders in controls (C) and AD patients (D). Colors and line thickness indicate the dPTE values (lower and upper thresholds: [0.5086, 0.5108] and [0.5060, 0.5085] for the controls and AD, respectively), and arrows indicate the preferred direction of information flow. Thresholds were (arbitrarily) chosen to highlight the dominant patterns formed by the information flows between regions. L = left; R = right; $0.5 < $ dPTE ≤ 1 represents information flow from region X to region Y; $0 \leq$ dPTE < 0.5 represents information flow towards region X from region Y, with X forming the columns and Y the rows in the matrix. (For interpretation of the references to color in this figure legend, the reader is referred to the web version of this article.)
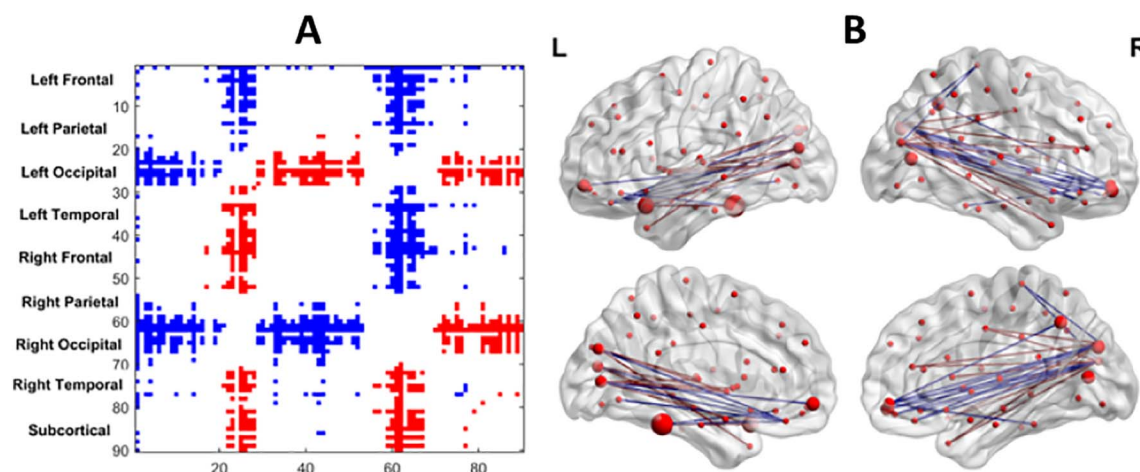
Fig. 3. Disrupted direction of information flow in AD patients in the beta band. (A) *p*-value ($p < 0.05$) matrix for each ROI showing significant between-group differences in directed connections between pairwise ROIs; permutation tests with FDR correction. (B) For visualization purposes, only a subset of the significantly different connections, namely those with $p < 0.0001$, between AD patients and controls is shown. Hot and cold colors indicate whether the strength of information flow (dPTE value) between pairs of brain regions was significantly higher or lower in controls than in AD patients, respectively. The details of information flow between specific regions are shown Table S2. (For interpretation of the references to color in this figure legend, the reader is referred to the web version of this article.)

ORBmid.R), temporal regions (TPOsup.R, TPOsup.L, TPOmid.R, TPOmid.L), limbic regions (ACG.R, MCG.R) and subcortical regions (AMYG.L, CAU.R, CAU.L, PUT.L, PAL.L, THA.L). The most significant connections with higher dPTE values in AD patients were located mostly in frontal regions (REC.L, REC.R, ORBsup.L, ORBsup.R, ORBsupmed.L, ORBsubmed.R, ORBmid.R, ORBinf.L, ORBinf.R, IFGtriang.L) and temporal regions (STG.L, TPOsup.L, TPOmid.L) but also in two central regions (PreCG.L, PCL.R), one limbic region (MCG.L), one insular region (INS.L) and one posterior region (SMG.L) and connected mainly to occipital regions (SOG.L, SOG.R, MOG.L, MOG.R, CAL.L, CUN.L, CUN.R, LING.L), but also to two posterior regions (PCUN.R, ANG.R) and two temporal regions (FFG.L, FFG.R). See Table S2 and Fig. S4 for details.

3.4. Correlations with cognition and CSF amyloid and tau

Spearman correlations revealed several correlations between the dPTE of each of the 90 AAL regions and MMSE, CSF tau and ptau and CSF amyloid. This revealed a positive correlation between MMSE and dPTE in the SMG.R region, and a negative correlation between MMSE and dPTE in the PreCG.L, ROL.L and IFGtriang.R regions. CSF ptau showed a negative correlation with dPTE in HIP.L, and CSF both tau and ptau showed negative correlations with dPTE in PCG.L and PCG. R. However, after FDR correction for multiple testing none of these correlations survived (Fig. S2 and Table S3).

4. Discussion

We hypothesized that the dominant posterior-to-anterior pattern of information flow would be disrupted in AD patients. In particular, we expected that in higher frequency bands the outflow from posterior regions would be reduced due to damage in posterior hub regions, and that in the theta band the outflow from the hippocampi would be reduced. Using resting-state MEG data for patients with AD and healthy controls, we studied these hypotheses using the dPTE as a measure of the direction of information flow in large-scale brain networks involving the cortical and subcortical regions. Our hypothesis was confirmed for the posterior regions. We found that the posterior-to-anterior pattern of information flow in the beta band, dominated by the visual cortex and posterior DMN in the controls, was decreased in patients with AD. In this band, the posterior regions in AD patients were less sending, and the pre-frontal regions were less receiving, than in controls. The information flow from the precuneus and the visual cortex

was in particular affected in AD, as well as the information flow towards subcortical structures. We did not find any group differences in other frequency bands, including the theta band where we found a preserved characteristic anterior-to-posterior pattern in AD patients.

4.1. Patterns of information flow

The patterns of information flow between cortical regions observed in the controls were similar to those reported using a different cohort of healthy individuals (Hillebrand et al., 2016a), despite the inclusion of sub-cortical regions in the present study. In the healthy subjects we found a posterior-to-anterior pattern of information flow in the higher frequency bands (lower alpha, beta) and an opposite directional pattern of information flow in the theta band. The disruption of posterior-to-anterior information flow in AD patients in the beta band was not only shown by comparing regional dPTE values between AD patients and controls, but also quantified by the lower PAx index in AD patients. Of note, the observed group difference in PAx values between AD and HC were mainly due to the different directions of central-to-posterior information flow (as quantified by CPx values) between the two groups. Moreover, because of the disruption of posterior regions in AD patients, the information flow from central regions to posterior and anterior regions in AD patients became more apparent than in the healthy controls. In addition, the changes observed for the AD in the posterior-to-anterior beta band pattern were in line with two previous studies based on EEG (Babiloni et al., 2009; Dauwan et al., 2016), although Dauwan et al. (2016) found these changes for both the alpha and beta band, whereas we only observed significant differences in the beta band. These differences could possibly be due to differences in patient cohort, MEG versus EEG, or source-level versus sensor-level analysis.

4.2. Hubs and direction of information flow

Fig. 2A, B shows that the mean dPTE values in AD are more centered around the equilibrium value of 0.5, suggesting that the posterior regions are less sending and frontal regions are less receiving compared to controls. A recent modeling study suggest that the balance of information flow depends on the hubness (measured by degree in this case) of a region, which high degree nodes being stronger senders (Stam et al., 2016). Moreover, strongly active hub regions seem to be particularly vulnerable in a neurodegenerative network model (de Haan et al., 2012). These modeling results, together with the often reported damage to posterior hub regions in AD and subsequent increase in

hubness in other, more anterior located, regions (Engels et al., 2015), may explain our observed disrupted pattern of information flow. These observations are congruent with the cascading-hub hypothesis, namely that signals are redirected when a hub fails, and the "next hub in line" gets more of the load. Therefore, if typical hub regions decline then other regions become more hub-like (Stam, 2014).

A study by Moon et al. (2015) reported the opposite relation between hubness of brain regions and the direction of information flow between them. However, this difference is most likely due to the use of a directed connectivity measure that is based on phase differences (rather than phase transfer entropy), as we have recently shown that such measures can give erroneous estimates of direction of information flow (Hillebrand et al., 2016a).

4.3. Hippocampal information flow

We found altered information flow in AD not only between cortical regions but also with subcortical regions. Previous MEG studies have shown that subcortical brain activity can be estimated using beamforming (Engels et al., 2016; Tenney et al., 2013; Hillebrand et al., 2016b). Since the hippocampi play a key role in AD pathology (Hampel et al., 2008), and are also hub regions in the AD functional networks (Battaglia et al., 2011), we hypothesized that information flow would be impaired for these regions. However, we were not able to detect differences in information flow between the groups with regard to the hippocampi. One reason for this could be reduced signal-to-noise ratio (SNR), and therefore lower spatial resolution for deeper regions (Hillebrand and Barnes, 2002). This may explain why a decreased information flow from the occipital regions towards the amygdala, a brain area that is not typically involved in AD, but has a close proximity to the hippocampi, was found. Despite the successful placements of virtual electrodes in previous studies (Engels et al., 2016; Hillebrand et al., 2016b), interpretation of time series reconstructed for a deeper region should be made with care since the presumed activity can actually arise from a broader area around the virtual electrode (Attal and Schwartz, 2013; Wennberg and Cheyne, 2014). Thus, hippocampal changes in information flow may simply be missed due to low SNR, and/or the interference of surrounding sources on the reconstructed time series. Another reason might be that hippocampal pathology did not change the information flow with the hippocampi. However, after calculating Spearman correlation coefficients between dPTE values in all regions with MMSE, CSF Aβ42, tau and ptau, we found a negative correlation in the left hippocampus between CSF ptau and dPTE. Although this correlation was not significant after correction for multiple comparisons this might hint to mechanisms that cause a pathological flow in the hippocampi. Future studies should focus on determining the relationship between disturbed information flow and pathological hallmarks in AD.

4.4. Memory component alterations in AD

Our results show that the sending properties of the posterior brain region and the receiving properties of the anterior brain region are altered in AD. This finding is in agreement with previous research showing DMN dysfunction regarding the anterior-posterior integration in AD (Greicius et al., 2004; Toussaint et al., 2014). The observation of a dominant posterior-to-anterior flow in the higher frequency range and an anterior-to-posterior flow in the lower frequency range is suggestive for a loop through which information circulates (Hillebrand et al., 2016a). This circulation seems to be disrupted in AD, but only for the posterior-to-anterior pattern in the higher frequency range. This may seem counterintuitive since the theta band is involved in memory processes in frontal areas and the hippocampi (Tóth et al., 2014). However, lack of differences in the theta band between AD patients and controls can possibly be explained by the relatively young age of the included patients. It is often reported that AD has a clinically distinct

presentation at a young age compared to late-onset AD, where early onset patients have fewer memory impairments (van der Flier et al., 2011).

4.5. Disruption in the beta band

We reported disruption of information flow between posterior and frontal regions, and between posterior and subcortical regions in AD in the beta band. The beta band is altered in many neurodegenerative disorders (Hughes and Rowe, 2013; Holschneider and Leuchter, 1995). However, with regard to functional connectivity, other frequency bands have also been reported to be altered in AD using MEG (Alonso et al., 2011; Escudero et al., 2011; Franciotti et al., 2006; Stam et al., 2002, 2006, 2009). Overall, the most powerful beta band activity in resting subjects is located in central brain areas, especially around the motor cortex in AD (Engels et al., 2016), which is thought to be a higher harmonic component of the rolandic mu-rhythm (for a review, see Hari and Salmelin, 1997). Interestingly, in a previous study on the same dataset (Engels et al., 2016), we reported that primary cortices are spared in AD in terms of slowing of relative power, which seems to be in concordance with the findings in the present study of a preserved information flow for these regions. In the supplemental material we show the correlations between dPTE values and relative power values in all frequency bands (Fig. S1, Fig. S5 and Fig. S6). Within the groups, the patterns of relative power were similar to those obtained for the dPTE (compare Fig. 1 and Fig. S1 to Fig. S5a), which is in accordance with the findings of Hillebrand et al. (2016a, 2016b). Although the beta band showed a significant positive correlation between relative power and dPTE values, so did other frequency bands for which there were no significant group differences in dPTE values (Fig. S6). Furthermore, the beta band showed more widespread significant group differences for relative power than for dPTE (compare Fig. 1 to Fig. S5a). This might suggest that the observed differences in dPTE cannot be fully explained by the group differences in relative power. However, one should take into account that this result does not guarantee a true independent relationship between dPTE and relative power values. For instance, the relative power and signal-to-noise ratios are different for each frequency band (Fig. S5b). This may affect phase estimates (Muthukumaraswamy and Singh, 2011) and dPTE estimates (although dPTE is relatively insensitive to SNR (Lobier et al., 2014), and therefore affect the ability to detect group differences for dPTE at low SNRs (i.e. within the constraints of inferential statistics, a non-significant difference does not necessarily equate the absence of a difference). Hence, although these results suggest that power differences are not the main driver of dPTE differences, we cannot fully rule out such an effect.

Activity in the beta band has also been associated with synchronization of long-distance interactions between brain regions (Kopell et al., 2000). In patients with AD, the functional connectivity in the beta band is frequently reported to be altered (Alonso et al., 2011; Stam et al., 2002, 2006, 2009). These studies together suggest a key role for the beta band to preserve long-range anterior-to-posterior functional connections, which might be vulnerable in AD patients.

4.6. Correlations with cognition and CSF biomarkers

Spearman correlation coefficients between regional dPTE values and MMSE and CSF biomarkers (Aβ42, tau and ptau) for the AD group were not significant after correction for multiple comparisons using FDR. However, the uncorrected significant correlations revealed trends in several regions (Table S3). In AD, Aβ42 levels in the CSF are typically decreased while tau and ptau levels are elevated (Mulder et al., 2010; Duits et al., 2014; Scheltens et al., 2016). On the other hand, MMSE scores are generally low in AD. With respect to the findings of decreased dPTE values in the beta band for the posterior region in AD, one could expect a positive correlation between the dPTE in those regions and MMSE. Indeed, we found a positive correlation for the SMG.R region.

The opposite pattern could be expected for the frontal regions, which was indeed the case for PreCG.L, ROL.L and IFGtriang.R. Thus, although these correlations with MMSE did not survive a multiple comparison correction, the correlations show a trend in the expected direction. The CSF biomarkers showed correlations with dPTE for several AD-related areas of which the left hippocampus (HIP.L) and left and right posterior cingulate gyri (PCG.L and PCG.R) stood out the most. HIP.L showed a negative correlation with CSF ptau, and PCG.L and PCG.R showed a positive correlation with both CSF tau and ptau. However, these correlations are not easy to understand since both biomarkers are typically elevated in AD, while a decrease in dPTE values in the posterior regions was observed. Therefore, a negative correlation was expected. For the hippocampi, no differences in dPTE values were found and therefore, the negative correlation with CSF ptau would suggest an increase of hippocampal information outflow. These observations provide a possible link between hippocampal information flow alterations and CSF biomarkers in AD patients.

4.7. Methodological considerations

We used a beamformer-based approach to reconstruct source-level brain activity, not only in cortical regions, but also in deeper subcortical structures. This allows for drawing more disease- and area-related conclusions. With regard to the statistical testing, the applied permutation tests combined with FDR correction (Benjamini and Hochberg, 1995) provide reliable statistical results (Ludbrook, 1994). However, this study also has a limitation that deserves consideration. The FDR (BHFDR; Benjamini and Hochberg, 1995) was controlled at an alpha level of 5%, and therefore 5% of the significant ROIs could still be false positive results. Furthermore, our results may have been influenced by methodological choices such as the selection of artifact-free epochs. An independent researcher (IN, in acknowledgements) double-checked our selected epochs to ensure the epoch quality, with no artifacts or signs of drowsiness.

5. Conclusion

In conclusion, we found a disrupted posterior-to-anterior pattern in AD in the beta band involving both cortical and subcortical brain regions. Most prominently, the information flow from the precuneus and the visual cortex, towards frontal and subcortical structures, was disrupted in AD. We conclude that AD pathology may affect the flow of information between brain regions, particularly from posterior hub regions, and that changes in the information flow in the beta band indicate an aspect of the pathophysiological process in AD.

Acknowledgements

Appendix A. Supplementary data

Supplementary data to this article can be found online at http://dx.doi.org/10.1016/j.nicl.2017.06.025.

References

Alonso, J.F., Poza, J., Mañanas, M.A., Romero, S., Fernández, A., Hornero, R., 2011. MEG connectivity analysis in patients with Alzheimer's disease using cross mutual information and spectral coherence. Ann. Biomed. Eng. 39 (1), 524–536.

Attal, Y., Schwartz, D., 2013. Assessment of subcortical source localization using deep brain activity imaging model with minimum norm operators: a MEG study. PLoS One 8 (3), e59856.

Babiloni, C., Ferri, R., Binetti, G., Vecchio, F., Frisoni, G.B., Lanuzza, B., Miniussi, C., Nobili, F., Rodriguez, G., Rundo, F., Cassarino, A., Infarinato, F., Cassetta, E., Salinari, S., Eusebi, F., Rossini, P.M., 2009. Directionality of EEG synchronization in Alzheimer's disease subjects. Neurobiol. Aging 30 (1), 93–102.

Baillet, S., Mosher, J.C., Leahy, R.M., 2001. Electromagnetic brain mapping. IEEE Signal Process. Mag. 18 (6), 14–30.

Battaglia, F.P., Benchenane, K., Sirota, A., Pennartz, C.M., Wiener, S.I., 2011. The hippocampus: hub of brain network communication for memory. Trends Cogn. Sci. 15 (7), 310–318.

Benjamini, Y., Hochberg, Y., 1995. Controling the false discovery rate: a practical and powerful approach to multiple testing. J. R. Stat. Soc. Ser. B Methodol. 57, 289–300.

Berendse, H.W., Verbunt, J.P., Scheltens, P., van Dijk, B.W., Jonkman, E.J., 2000. Magnetoencephalographic analysis of cortical activity in Alzheimer's disease: a pilot study. Clin. Neurophysiol. 111 (4), 604–612.

Besthorn, C., Förstl, H., Geiger-Kabisch, C., Sattel, H., Gasser, T., Schreiter-Gasser, U., 1994. EEG coherence in Alzheimer disease. Electroencephalogr. Clin. Neurophysiol. 90 (3), 242–245.

Cheyne, D., Bostan, A.C., Gaetz, W., Pang, E.W., 2007. Event-related beamforming: a robust method for presurgical functional mapping using MEG. Clin. Neurophysiol. 118 (8), 1691–1704.

Corsi-Cabrera, M., Galindo-Vilchis, L., del-Río-Portilla, Y., Arce, C., Ramos-Loyo, J., 2007. Within-subject reliability and inter-session stability of EEG power and coherent activity in women evaluated monthly over nine months. Clin. Neurophysiol. 118 (1), 9–21.

Crossley, N.A., Mechelli, A., Scott, J., Carletti, F., Fox, P.T., McGuire, P., Bullmore, E.T., 2014. The hubs of the human connectome are generally implicated in the anatomy of brain disorders. Brain 137 (Pt 8), 2382–2395.

Dauwan, M., van Dellen, E., van Boxtel, L., van Straaten, E.C.W., de Waal, H., Lemstra, A.W., Gouw, A.A., van der Flier, W.M., Scheltens, P., Sommer, I.E., Stam, C.J., 2016. EEG-directed connectivity from posterior brain regions is decreased in dementia with Lewy bodies: a comparison with Alzheimer's disease and controls. Neurobiol. Aging 14, 122–129.

van Diessen, E., Numan, T., van Dellen, E., van der Kooi, A.W., Boersma, M., Hofman, D., van Lutterveld, R., van Dijk, B.W., van Straaten, E.C., Hillebrand, A., Stam, C.J., 2015. Opportunities and methodological challenges in EEG and MEG resting state functional brain network research. Clin. Neurophysiol. 126 (8), 1468–1481.

Duits, F.H., Teunissen, C.E., Bouwman, F.H., Visser, P.J., Mattsson, N., Zetterberg, H., Blennow, K., Hansson, O., Minthon, L., Andreasen, N., Marcusson, J., Wallin, A., Rikkert, M.O., Tsolaki, M., Parnetti, L., Herukka, S.K., Hampel, H., de Leon, M.J., Schröder, J., Aarsland, D., Blankenstein, M.A., Scheltens, P., van der Flier, W.M., 2014. The cerebrospinal fluid "Alzheimer profile": easily said, but what does it mean? Alzheimers Dement. 10 (6), 713–723.e2.

Duits, F.H., Prins, N.D., Lemstra, A.W., Pijnenburg, Y.A., Bouwman, F.H., Teunissen, C.E., Scheltens, P., van der Flier, W.M., 2015. Diagnostic impact of CSF biomarkers for Alzheimer's disease in a tertiary memory clinic. Alzheimers Dement. 11 (5), 523–532.

Engels, M.M., Stam, C.J., van der Flier, W.M., Scheltens, P., de Waal, H., van Straaten, E.C.W., 2015. Declining functional connectivity and changing hub locations in Alzheimer's disease: an EEG study. BMC Neurol. 20, 15–145.

Engels, M.M., Hillebrand, A., van der Flier, W.M., Stam, C.J., Scheltens, P., van Straaten, E.C.W., 2016. Slowing of hippocampal activity correlates with cognitive decline in early onset Alzheimer's disease. An MEG study with virtual electrodes. Front. Hum. Neurosci. 10, 238.

Engels, M.M.A., van der Flier, W.M., Stam, C.J., Hillebrand, A., Scheltens, P., van Straaten, E.C.W., 2017. Alzheimer's disease: The state of the art in resting-state magnetoencephalography. Clin. Neurophysiol. 128 (8), 1426–1437.

Escudero, J., Sanei, S., Jarchi, D., Abásolo, D., Hornero, R., 2011. Regional coherence evaluation in mild cognitive impairment and Alzheimer's disease based on adaptively extracted magnetoencephalogram rhythms. Physiol. Meas. 32 (8), 1163–1180.

van der Flier, W.M., Pijnenburg, Y.A.L., Fox, N.C., Scheltens, P., 2011. Early-onset versus late-onset Alzheimer's disease: the case of the missing APOE ε4 allele. Lancet 10, 280e288.

van der Flier, W.M., Pijnenburg, Y.A., Prins, N., Lemstra, A.W., Bouwman, F.H., Teunissen, C.E., van Berckel, B.N., Stam, C.J., Barkhof, F., Visser, P.J., van Egmond, E., Scheltens, P., 2014. Optimizing patient care and research: the Amsterdam Dementia Cohort. J. Alzheimers Dis. 41 (1), 313–327.

Franciotti, R., Iacono, D., Della Penna, S., Pizzella, V., Torquati, K., Onofrj, M., Romani, G.L., 2006. Cortical rhythms reactivity in AD, LBD and normal subjects: a quantitative MEG study. Neurobiol. Aging 27 (8), 1100–1109.

Friston, K.J., 2011. Functional and effective connectivity: a review. Brain Connect. 1 (1), 13–36.

Gong, G., He, Y., Concha, L., Lebel, C., Gross, D.W., Evans, A.C., Beaulieu, C., 2009. Mapping anatomical connectivity patterns of human cerebral cortex using in vivo diffusion tensor imaging tractography. Cereb. Cortex 19 (3), 524–536.

Greicius, M.D., Srivastava, G., Reiss, A.L., Menon, V., 2004. Default-mode network activity distinguishes Alzheimer's disease from healthy aging: evidence from functional MRI. Proc. Natl. Acad. Sci. U. S. A. 101 (13), 4637–4642.

Guevara, R., Velazquez, J.L., Nenadovic, V., Wennberg, R., Senjanovic, G., Dominguez,

L.G., 2005. Phase synchronization measurements using electroencephalographic recordings: what can we really say about neuronal synchrony? Neuroinformatics 3 (4), 301–314.

de Haan, W., Mott, K., van Straaten, E.C., Scheltens, P., Stam, C.J., 2012. Activity dependent degeneration explains hub vulnerability in Alzheimer's disease. PLoS Comput. Biol. 8 (8), e1002582.

Hampel, H., Bürger, K., Teipel, S.J., Bokde, A.L., Zetterberg, H., Blennow, K., 2008. Core candidate neurochemical and imaging biomarkers of Alzheimer's disease. Alzheimers Dement. 4 (1), 38–48.

Hari, R., Salmelin, R., 1997. Human cortical oscillations: a neuromagnetic view through the skull. Trends Neurosci. 20 (1), 44–49.

Hillebrand, A., Barnes, G.R., 2002. A quantitative assessment of the sensitivity of whole-head MEG to activity in the adult human cortex. NeuroImage 16 (3 Pt 1), 638–650.

Hillebrand, A., Singh, K.D., Holliday, I.E., Furlong, P.L., Barnes, G.R., 2005. A new approach to neuroimaging with magnetoencephalography. Hum. Brain Mapp. 25 (2), 199–211.

Hillebrand, A., Barnes, G.R., Bosboom, J.L., Berendse, H.W., Stam, C.J., 2012. Frequency-dependent functional connectivity within resting-state networks: an atlas-based MEG beamformer solution. NeuroImage 59 (4), 3909–3921.

Hillebrand, A., Fazio, P., de Munck, J.C., van Dijk, B.W., 2013. Feasibility of clinical magnetoencephalography (MEG) functional mapping in the presence of dental artefacts. Clin. Neurophysiol. 124 (1), 107–113.

Hillebrand, A., Tewarie, P., van Dellen, E., Yu, M., Carbo, E.W.S., Douw, L., Gouw, A., van Straaten, E.C.W., Stam, C.J., 2016a. Direction of information flow in large-scale resting-state networks is frequency-dependent. Proc. Natl. Acad. Sci. U. S. A. 113 (14), 3867–3872.

Hillebrand, A., Nissen, I.A., Ris-Hilgersom, I., Sijsma, N.C., Ronner, H.E., van Dijk, B.W., Stam, C.J., 2016b. Detecting epileptiform activity from deeper brain regions in spatially filtered MEG data. Clin. Neurophysiol. 127 (8), 2766–2769.

Hlaváčková-Schindler, K., Paluš, M., Vejmelkab, M., Bhattacharyaa, J., 2007. Causality detection based on information-theoretic approaches in time series analysis. Phys. Rep. 441, 1–46.

Holschneider, D.P., Leuchter, A.F., 1995. Beta activity in aging and dementia. Brain Topogr. 8 (2), 169–180.

Hughes, L.E., Rowe, J.B., 2013. The impact of neurodegeneration on network connectivity: a study of change detection in frontotemporal dementia. J. Cogn. Neurosci. 25 (5), 802–813.

Kopell, N., Ermentrout, G.B., Whittington, M.A., Traub, R.D., 2000. Gamma rhythms and beta rhythms have different synchronization properties. Proc. Natl. Acad. Sci. U. S. A. 97 (4), 1867–1872.

Kullback, S., Leibler, R.A., 1951. On information and sufficiency. Ann. Math. Stat. 22 (1), 79–86.

Lobier, M., Siebenhühner, F., Palva, S., Palva, J.M., 2014. Phase transfer entropy: a novel phase-based measure for directed connectivity in networks coupled by oscillatory interactions. NeuroImage 85, 853–872.

Ludbrook, J., 1994. Advantages of permutation (randomization) test in clinical and experimental pharmacology and physiology. Clin. Exp. Pharmacol. Physiol. 21, 673e686.

McKhann, G.M., Knopman, D.S., Chertkow, H., Hyman, B.T., Jack Jr., C.R., Kawas, C.H., Klunk, W.E., Koroshetz, W.J., Manly, J.J., Mayeux, R., Mohs, R.C., Morris, J.C., Rossor, M.N., Scheltens, P., Carrillo, M.C., Thies, B., Weintraub, S., Phelps, C.H., 2011. The diagnosis of dementia due to Alzheimer's disease: recommendations from the National Institute on Aging-Alzheimer's Association workgroups on diagnostic guidelines for Alzheimer's disease. Alzheimers Dement. 7 (3), 263–269.

Medvedovsky, M., Taulu, S., Bikmullina, R., Ahonen, A., Paetau, R., 2009. Fine tuning the correlation limit of spatio-temporal signal space separation for magnetoencephalography. J. Neurosci. Methods 177 (1), 203–211.

Moon, J.Y., Lee, U., Blain-Moraes, S., Mashour, G.A., 2015. General relationship of global topology, local dynamics, and directionality in large-scale brain networks. PLoS Comput. Biol. 11 (4), e1004225.

Mulder, C., Verwey, N.A., van der Flier, W.M., Bouwman, F.H., Kok, A., van Elk, E.J., Scheltens, P., Blankenstein, M.A., 2010. Amyloid-beta(1-42), total tau, and phosphorylated tau as cerebrospinal fluid biomarkers for the diagnosis of Alzheimer disease. Clin. Chem. 56, 248e253.

Muthukumaraswamy, S.D., Singh, K.D., 2011. A cautionary note on the interpretation of phase-locking estimates with concurrent changes in power. Clin. Neurophysiol. 122 (11), 2324–2325.

Paluš, M., Stefanovska, A., 2003. Direction of coupling from phases of interacting oscillators: an information-theoretic approach. Phys. Rev. E 67, 055201(R).

Paluš, M., Vejmelka, M., 2007. Directionality of coupling from bivariate time series: how to avoid false causalities and missed connections. Phys. Rev. E 75, 056211.

Prokopenko, M., Lizier, J.T., 2014. Transfer entropy and transient limits of computation. Sci Rep 4, 5394.

Robinson, S.E., Vrba, J., 1999. Functional Neuroimaging by Synthetic Aperture Magnetometry (SAM). Recent Advances in Biomagnetism. Tohoku Univ. Press, Sendai, Japan, pp. 302–305.

Rosenblum, M.G., Pikovsky, A.S., Kurths, J., 1996. Phase synchronization of chaotic oscillators. Phys. Rev. Lett. 76 (11), 1804–1807.

Rosenblum, M.G., Pikovsky, A.S., Kurths, J., Schäfer, C., Tass, P., 2001. Phase synchronization: from theory to data analysis. In: Hoff, A.J. (Ed.), Neuro-informatics and Neural Modeling, Handbook of Biological Physics. Vol 4. Elsevier, New York, pp. 279–321.

Scheltens, P., Blennow, K., Breteler, M.M., de Strooper, B., Frisoni, G.B., Salloway, S., van der Flier, W.M., 2016. Alzheimer's disease. Lancet 388 (10043), 505–517.

Schreiber, T., 2000. Measuring information transfer. Phys. Rev. Lett. 8, 5461–5464.

Sekihara, K., Nagarajan, S.S., Poeppel, D., Marantz, A., 2004. Asymptotic SNR of scalar and vector minimum-variance beamformers for neuromagnetic source reconstruction. IEEE Trans. Biomed. Eng. 51 (10), 1726–1734.

Shannon, C.E., 1948. A mathematical theory of communication. Bell Syst. Tech. J. 27 (3), 379–423.

Stam, C.J., 2014. Modern network science of neurological disorders. Nat. Rev. Neurosci. 15 (10), 683–695.

Stam, C.J., van Cappellen van Walsum, A.M., Pijnenburg, Y.A., Berendse, H.W., de Munck, J.C., Scheltens, P., van Dijk, B.W., 2002. Generalized synchronization of MEG recordings in Alzheimer's disease: evidence for involvement of the gamma band. J. Clin. Neurophysiol. 19 (6), 562–574.

Stam, C.J., Jones, B.F., Manshanden, I., van Cappellen van Walsum, A.M., Montez, T., Verbunt, J.P., de Munck, J.C., van Dijk, B.W., Berendse, H.W., Scheltens, P., 2006. Magnetoencephalographic evaluation of resting-state functional connectivity in Alzheimer's disease. NeuroImage 32 (3), 1335–1344.

Stam, C.J., de Haan, W., Daffertshofer, A., Jones, B.F., Manshanden, I., van Cappellen van Walsum, A.M., Montez, T., Verbunt, J.P., de Munck, J.C., van Dijk, B.W., Berendse, H.W., Scheltens, P., 2009. Graph theoretical analysis of magnetoencephalographic functional connectivity in Alzheimer's disease. Brain 132 (Pt1), 213–224.

Stam, C.J., van Straaten, E.C., van Dellen, E., Tewarie, P., Gong, G., Hillebrand, A., Meier, J., van Mieghem, P., 2016. The relation between structural and functional connectivity patterns in complex brain networks. Int. J. Psychophysiol. 103, 149–160.

Staniek, M., Lehnertz, K., 2008. Symbolic transfer entropy. Phys. Rev. Lett. 18;100 (15), 158101.

Taulu, S., Hari, R., 2009. Removal of magnetoencephalographic artifacts with temporal signal-space separation: demonstration with single-trial auditory-evoked responses. Hum. Brain Mapp. 30 (5), 1524–1534.

Taulu, S., Simola, J., 2006. Spatiotemporal signal space separation method for rejecting nearby interference in MEG measurements. Phys. Med. Biol. 51 (7), 1759–1768.

Tenney, J.R., Fujiwara, H., Horn, P.S., Jacobson, S.E., Glauser, T.A., Rose, D.F., 2013. Focal corticothalamic sources during generalized absence seizures: a MEG study. Epilepsy Res. 106 (1–2), 113–122.

Teunissen, C.E., Petzold, A., Bennett, J.L., Berven, F.S., Brundin, L., Comabella, M., Franciotta, D., Frederiksen, J.L., Fleming, J.O., Furlan, R., Hintzen, R.Q., Hughes, S.G., Johnson, M.H., Krasulova, E., Kuhle, J., Magnone, M.C., Rajda, C., Rejdak, K., Schmidt, H.K., van Pesch, V., Waubant, E., Wolf, C., Giovannoni, G., Hemmer, B., Tumani, H., Deisenhammer, F., 2009. A consensus protocol for the standardization of cerebrospinal fluid collection and biobanking. Neurology 73 (22), 1914–1922.

Tóth, B., Kardos, Z., File, B., Boha, R., Stam, C.J., Molnár, M., 2014. Frontal midline theta connectivity is related to efficiency of WM maintenance and is affected by aging. Neurobiol. Learn. Mem. 114, 58–69.

Toussaint, P.J., Maiz, S., Coynel, D., Doyon, J., Messé, A., de Souza, L.C., Sarazin, M., Perlbarg, V., Habert, M.O., Benali, H., 2014. Characteristics of the default mode functional connectivity in normal ageing and Alzheimer's disease using resting state fMRI with a combined approach of entropy-based and graph theoretical measurements. NeuroImage 101, 778e786.

Tzourio-Mazoyer, N., Landeau, B., Papathanassiou, D., Crivello, F., Etard, O., Delcroix, N., Mazoyer, B., Joliot, M., 2002. Automated anatomical labeling of activations in SPM using a macroscopic anatomical parcellation of the MNI MRI single-subject brain. NeuroImage 15 (1), 273–289.

van Veen, B.D., van Drongelen, W., Yuchtman, M., Suzuki, A., 1997. Localization of brain electrical activity via linearly constrained minimum variance spatial filtering. IEEE Trans. Biomed. Eng. 44 (9), 867–880.

Verhage, F., 1964. Intelligence and Age: Study With Dutch People Aged 12 to 77. (in Dutch).

Wang, K., Liang, M., Wang, L., Tian, L., Zhang, X., Li, K., Jiang, T., 2007. Altered functional connectivity in early Alzheimer's disease: a resting-state fMRI study. Hum. Brain Mapp. 28 (10), 967–978.

Wennberg, R., Cheyne, D., 2014. Reliability of MEG source imaging of anterior temporal spikes: analysis of an intracranially characterized spike focus. Clin. Neurophysiol. 125, 903–918.

Whalen, C., Maclin, E.L., Fabiani, M., Gratton, G., 2008. Validation of a method for coregistering scalp recording locations with 3D structural MR images. Hum. Brain Mapp. 29 (11), 1288–1301.

Wibral, M., Rahm, B., Rieder, M., Lindner, M., Vicente, R., Kaiser, J., 2011. Transfer entropy in magnetoencephalographic data: quantifying information flow in cortical and cerebellar networks. Prog. Biophys. Mol. Biol. 105 (1–2), 80–97.

Yu, M., Engels, M.M.A., Hillebrand, A., van Straaten, E.C., Gouw, A.A., Teunissen, C., van der Flier, W.M., Scheltens, P., Stam, C.J., 2017. Selective impairment of hippocampus and posterior hub areas in Alzheimer's disease: an MEG-based multiplex network study. Brain 140 (5), 1466–1485.

Zhang, H.Y., Wang, S.J., Xing, J., Liu, B., Ma, Z.L., Yang, M., Zhang, Z.J., Teng, G.J., 2009. Detection of PCC functional connectivity characteristics in resting-state fMRI in mild Alzheimer's disease. Behav. Brain Res. 197 (1), 103–108.